UCRL-JC-133349
PREPRINT

High-Field Electron-Photon Interactions

F. V. Hartemann, H. A. Baldis, A. K. Kerman, E. C. Landahl,
N. C. Luhmann, Jr., A. L. Troha, J. R. Van Meter

This paper was prepared for submittal to the
Proceedings of the International Conference on Lasers
Tucson, AZ
March 19-21, 1998

February 26, 1999

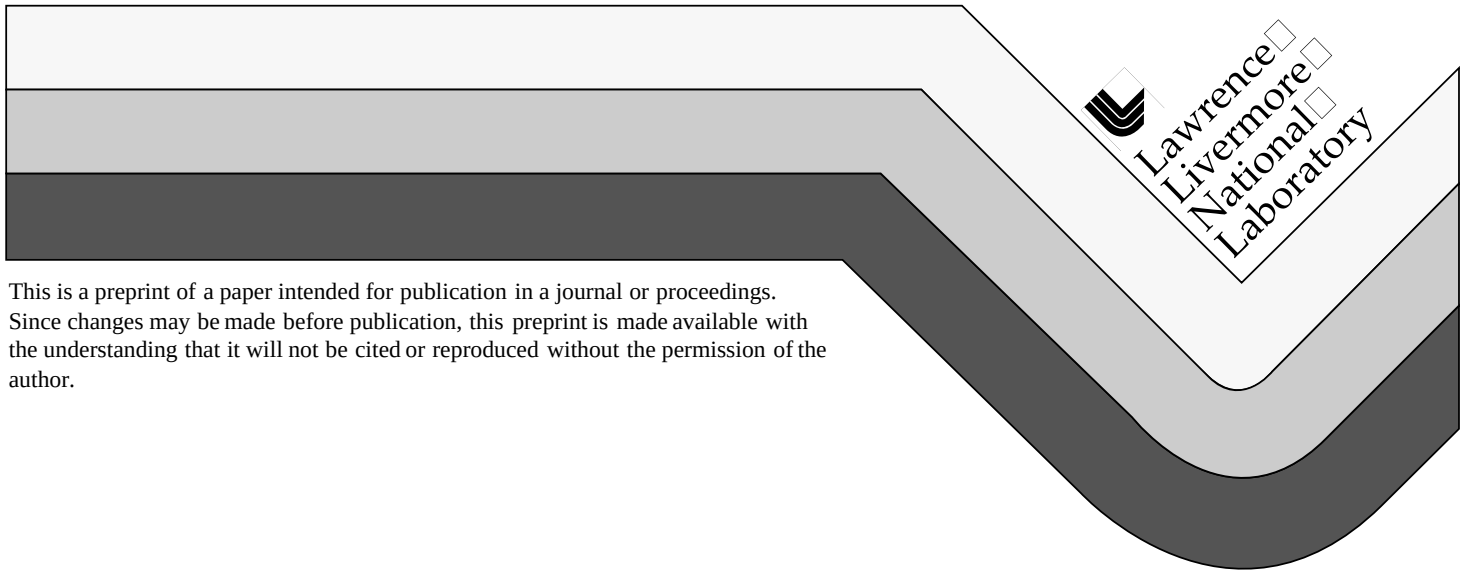

UCRL-JC-133349

HIGH-FIELD ELECTRON-PHOTON INTERACTIONS

F.V. Hartemann,[a,b] H.A. Baldis,[a,b] A.K. Kerman,[c] E.C. Landahl,[a,b]
N.C. Luhmann, Jr.,[b] A.L. Troha,[a,b]
J.R. Van Meter,[a,d]

[a]Institute for Laser Science and Applications,
Lawrence Livermore National Laboratory, Livermore, CA 94550
[b]Department of Applied Science, University of California, Davis, CA 95616
[c]Centre for Theoretical Physics and Physics Department, Massachusetts Institute of Technology, Cambridge, MA 02139
[d]Department of Physics, University of California, Davis, CA 95616

Abstract

Recent advances in novel technologies (including chirped-pulse amplification, femtosecond laser systems operating in the TW-PW range, high-gradient rf photoinjectors, and synchronized relativistic electron bunches with subpicosecond durations and THz bandwidths) allow experimentalists to study the interaction of relativistic electrons with ultrahigh-intensity photon fields. Ponderomotive scattering can accelerate these electrons with extremely high gradients in a three-dimensional vacuum laser focus. The nonlinear Doppler shift induced by relativistic radiation pressure in Compton backscattering is shown to yield complex nonlinear spectra which can be modified by using temporal laser pulse shaping techniques. Colliding lasers pulses, where ponderomotive acceleration and Compton backscattering are combined, could also yield extremely short wavelength photons. Finally, one expects strong radiative corrections when the Doppler-upshifted laser wavelength approaches the Compton scale. These are discussed within the context of high-field classical electrodynamics, a new discipline borne out of the aforementioned innovations.

Introduction

The physics of laser-electron interactions changes dramatically at relativistic intensities, where the transverse momentum of the charge in the laser wave, as measured in electron units, exceeds unity. Three fundamental vacuum processes are know to occur in this regime: relativistic ponderomotive scattering,[1] ultrahigh-intensity Compton backscattering,[2,3] and nonlinear Kapitza-Dirac scattering.[4,5]

A detailed knowledge of the 3D electromagnetic field distribution of the focusing laser wave is needed to study high-intensity scattering and properly model experimental results. For example, two ultrahigh-intensity relativistic electron scattering experiments are currently underway at SLAC and CEA. In the first case, nonlinear (multiphoton) Compton backscattering is investigated using the SLAC 50 GeV beam and a tightly focused TW-class laser;[6] at CEA, low-energy electrons are accelerated by a TW laser.[7] In both instances, the 3D nature of the focused laser pulse is an essential feature of the experiment and must be described accurately to interpret the resulting data correctly.

In this paper, we present a extensive theoretical and numerical description of the relativistic dynamics of a charged particle interacting with an external electromagnetic field propagating *in vacuo*. To correctly describe the focusing and diffraction of the drive laser in vacuum, the paraxial propagator approach is used, where the mass-shell condition (vacuum dispersion relation) is approximated by a quadratic Taylor expansion in the 4-wavenumber. This approach is extremely accurate for any realizable laser focus, and gives analytic solutions for the fields. Also, the gauge condition is exactly satisfied everywhere, thus yielding a proper treatment of the axial electromagnetic field components due to wavefront curvature. The electron phase is used as the independent variable, thus allowing for particle tracking over an arbitrarily large number of Rayleigh ranges, independent of the nonlinear slippage and relativistic Doppler shift due to radiation pressure. The scattering of radiation by the accelerated electron is also reviewed, in the case of plane electromagnetic waves of arbitrary intensity, and radiative corrections are briefly discussed in the context of the classical Dirac-Lorentz equation. Finally, coherent harmonic generation is considered in the case of a laser modulated relativistic electron beam.

Lorentz-Maxwell Electrodynamics, Plane Wave Theory

Canonical Invariants

The electron 4-velocity and 4-momentum are defined as $u_\mu = d_\tau x_\mu$ and $p_\mu = m_0 c\, u_\mu$, with $u_\mu\, u^\mu = -1$. Here, τ is the proper time along the dimensionless electron world line $x_\mu(\tau)$. Neglecting radiative corrections,[2,8] the natural length scale of the problem is the laser wavelength, c/ω_0, while time is measured in units of $1/\omega_0$, charge in units of e, and mass in units of m_0. The energy-momentum transfer equations are given by the Lorentz force $d_\tau u_\mu = -(\partial_\mu A_\nu - \partial_\nu A_\mu)\, u^\nu$. For plane waves, the normalized 4-vector potential of the laser wave is $A_\mu(\phi) = [0, A(\phi)]$, where $\phi = k_\mu x^\mu(\tau)$ is the relativistically invariant phase of the traveling wave along the electron trajectory. Choosing $k_\mu = (1, 0, 0, 1)$, with the wave propagating in the z-direction, one has $d_\tau \phi = \gamma - u_z = \kappa$, which defines the light-cone variable κ, and the 4-momentum transfer equations read

$$d_\tau \boldsymbol{u}_\perp = \kappa\, d_\phi \boldsymbol{A}_\perp(\phi), \tag{1}$$

$$d_\tau u_z = d_\tau \gamma = \boldsymbol{u}_\perp \bullet d_\phi \boldsymbol{A}_\perp(\phi). \tag{2}$$

Equation (2) shows that κ is invariant: $\kappa = \kappa_0 = \gamma_0 (1 - \beta_0)$; also, Eq. (1) can be integrated to yield the transverse momentum invariant[9] $\boldsymbol{u}_\perp(\tau) = \boldsymbol{A}_\perp(\phi)$, and the energy and axial momentum are easily obtained since the 4-velocity is a unit 4-vector $\left(\gamma^2 = 1 + \boldsymbol{u}_\perp^2 + u_z^2\right)$:

$$u_z(\tau) = \gamma_0 \left[\beta_0 + \frac{1}{2}(1+\beta_0) A_\perp^2(\phi)\right], \tag{3}$$

$$\gamma(\tau) = \gamma_0 \left[1 + \frac{1}{2}(1+\beta_0) A_\perp^2(\phi)\right]. \tag{4}$$

The quadratic dependence of the energy and axial momentum on the normalized 4-vector potential denotes the relativistic scattering regime, where $A_\perp \geq 1$. Here, the ponderomotive force dominates the electron dynamics, yielding nonlinear slippage and Doppler shifts.[1,3] Equation (4) also provides a scaling for the maximum energy in a plane wave: $\gamma^*/\gamma_0 \simeq A_\perp^2$, for relativistic electrons. Finally, the electron position is given by $\boldsymbol{x}(\phi) = \frac{1}{\kappa_0} \int_{-\infty}^{\phi} \boldsymbol{u}(\psi)\, d\psi$.

Compton Scattering, Nonlinear Spectra

The focus of this section is the spectral characteristics of the radiation scattered by the accelerated charge. The distribution of energy radiated per unit solid angle, per unit frequency is derived[9] by considering the instantaneous radiated power, as described by the Larmor formula, and applying Parsival's theorem to obtain

$$\frac{d^2N(\varpi, \boldsymbol{n})}{d\varpi\, d\Omega} = \frac{a\varpi}{4\pi^2} \left| \int_{-\infty}^{+\infty} \boldsymbol{n} \times (\boldsymbol{n} \times \boldsymbol{\beta})\, \exp\left[i\, \varpi (t - \boldsymbol{n} \bullet \boldsymbol{x})\right] dt \right|^2, \tag{5}$$

where ϖ is the frequency measured in units of ω_0, and a is the fine structure constant. The quantity in Eq. (5) corresponds to the average radiated photon number. Using the phase as the independent variable, one now has

$$\frac{d^2N(\varpi, \boldsymbol{n})}{d\varpi\, d\Omega} = \frac{a\varpi}{4\pi^2 \kappa_0^2} \left| \int_{-\infty}^{+\infty} \boldsymbol{n} \times \left[\boldsymbol{n} \times \boldsymbol{u}(\phi)\right] \exp\left\{i\, \varpi \left[\phi + z(\phi) - \boldsymbol{n} \bullet \boldsymbol{x}(\phi)\right]\right\} d\phi \right|^2, \tag{6}$$

where the plane wave invariance of $\kappa = \kappa_0$ has been used.

An interesting case is the backscattered radiation, where most of the power is radiated and where one obtains the maximum relativistic Doppler upshift. Here, $\boldsymbol{n} = -\hat{z}$, $z(\phi) - \boldsymbol{n} \bullet \boldsymbol{x}(\phi) = 2\, z(\phi)$, $\hat{z} \times [\hat{z} \times \boldsymbol{u}(\phi)] = -\boldsymbol{A}_\perp(\phi)$, and Eq. (6) can now be recast in a manifestly covariant way, to read

$$\frac{d^2N(\varpi, -\hat{z})}{d\varpi\, d\Omega} = \frac{a}{4\pi^2}\, \chi \left| \int_{-\infty}^{+\infty} \boldsymbol{A}_\perp(\phi)\, \exp\left\{i\, \chi \left[\phi + \int_{-\infty}^{\phi} A_\perp^2(\psi)\, d\psi\right]\right\} d\phi \right|^2, \tag{7}$$

where the normalized Doppler-shifted frequency $\chi = \varpi\, (1+\beta_0)/(1-\beta_0)$ is used.

The functional dependence of the spectrum is now independent of β_0, which only sets the frequency scale. This comes directly from covariance: by changing the reference frame in which the scattering is viewed, one can vary the sign of β_0 and go

continuously from the FEL geometry[10] to the laser acceleration geometry.[11-16] For the FEL, the laser frequency is Doppler-upshifted, while it is downshifted in the second case. In both cases, the normalized vector potential and the average photon number are conserved as they are both Lorentz invariant.

Circular Polarization

Having derived the expression for the nonlinear backscattered light spectrum for arbitrary polarizations and intensities, we will now examine one important case: circularly polarized plane waves. Here, the dimensionless 4-vector potential can be expressed as $A_\perp(\phi) = A_0\, g(\phi)\, (\hat{x}\, \sin\phi + \hat{y}\, \cos\phi)$, which implies that the magnitude of the 4-vector potential varies adiabatically as the pulse intensity envelope: $A_\mu A^\mu = A_\perp^2(\phi) = A_0^2\, g^2(\phi)$. A simple physical model for the pulse envelope is a hyperbolic secant, i.e. $g(\phi) = \cosh^{-1}(\phi/\eta)$, so that the electron's axial position can be determined analytically.[17] Employing Eq. (7), the energy radiated per unit solid angle, per unit frequency can be derived analytically[3] for this case:

$$\frac{d^2N(\varpi,-\hat{z})}{d\varpi\, d\Omega} = \frac{\alpha A_0^2\, \eta^2\, \chi}{8}\left\{\left|\frac{\Phi(\mu_-, 1, 2\, i\, A_0^2\, \chi\, \eta)}{\cosh\left[\frac{\pi}{2}\,\eta\,(\chi-1)\right]}\right|^2 + \left|\frac{\Phi(\mu_+, 1, 2\, i\, A_0^2\, \chi\, \eta)}{\cosh\left[\frac{\pi}{2}\,\eta\,(\chi+1)\right]}\right|^2\right\}. \tag{8}$$

Here, Φ is the degenerate (confluent) hypergeometric function,[17] and $\mu_\pm = \frac{1}{2}\left[1 + i\,\eta\,(\chi \pm 1)\right]$. The electron dynamics are shown in Fig. 1 (left), while the behavior of the nonlinear spectral function is illustrated in Fig.1 (right) for $\eta = 5$, and different values of A_0. In this context, the onset of nonlinear relativistic spectral effects corresponds to a situation where the electron phase ϕ and the axial Doppler shift $\int_{-\infty}^{\phi} A_\perp^2(\psi)\, d\psi$ become comparable due to the intense radiation pressure of the drive laser pulse. This is directly related to the relativistic mass shift of the "dressed" electron in the ultrahigh-intensity laser pulse.

For linear polarization, the nonlinear effects are even stronger since there is an extra modulation of the axial velocity at the second harmonic of the laser, resulting from the $\mathbf{v} \times \mathbf{B}$ ponderomotive force (radiation pressure).

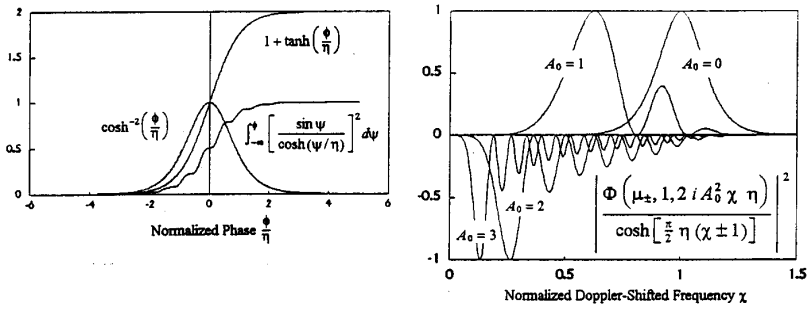

Fig. 1 Left: behavior of the normalized axial electron position for circular and linear polarizations. Right: nonlinear spectral function for circularly polarized light and different values of A_0. In both cases, $cosh^{-2}$ intensity envelope, $\eta = 5$.

Temporal Pulse Shaping

A very important result of the nonlinear Doppler effect described above resides in the fact that, at ultrahigh intensities, the peak photon number density in each line is nearly constant across the spectrum.[3] This indicates that for ultrashort laser pulses, even in the case of circularly polarized light, the backscattered energy is redistributed over a wide spectral range instead of contributing to a single, narrow, Compton backscattered line. This may be a serious difficulty for applications, such as the $\gamma - \gamma$ collider, which require the generation of a single, intense, highly collimated, narrow X-ray or γ-ray line.

This problem can be mitigated by shaping the temporal envelope of the pump laser pulse in order to minimize the change in the nonlinear Doppler shift during the interaction. In this scheme, as shown in Fig. 2 (left), the main part of the laser pulse is flat, which gives a constant axial electron velocity during most of the interaction. The associated Doppler shift thus remains nearly constant, resulting in the radiation of a narrow spectral line, as indicated in Fig. 2 (right). During the rise and the fall of the laser pulse, transient lines are radiated, but they are minimized by using this technique, which is rather analogous to the use of a tapered wiggler entrance in an FEL.[10]

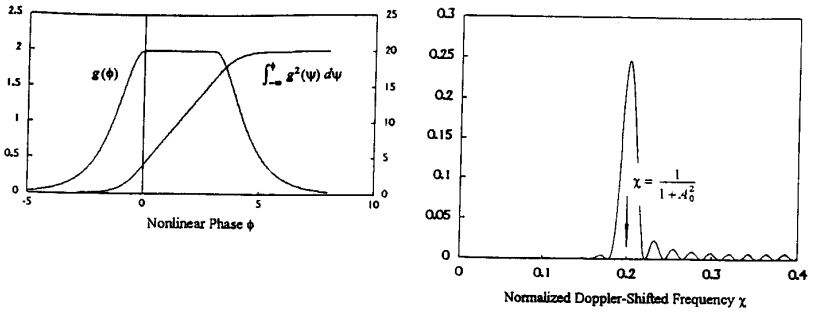

Fig. 2 Left: hyperbolic secant envelope with a flat-top, and axial electron position. Right: nonlinear spectrum for $A_0 = 2$, $\eta = 5$, $\theta = 10$.

To study the effects of pulse shaping on the Compton backscattered spectra in the nonlinear regime, and to find the optimum temporal profile of the laser pulse envelope, we introduce variable pulse shapes which are modeled theoretically by considering a circularly polarized pulse with a composite envelope, including a $cosh^{-1}$ rise and fall, and a constant flat-top: $g(\phi) = \cosh^{-1}(\phi/\eta)$ for $\phi \le 0$, $g(\phi) = 1$ for $0 \le \phi \le \theta$, and $g(\phi) = \cosh^{-1}\left(\frac{\phi-\theta}{\eta}\right)$ for $\phi \ge \theta$. The pulse shape is then parametrized by the ratio of the flat-top to the FWHM, which is equal to $\rho = \frac{\theta}{\theta + 2\eta \ln(2+\sqrt{3})}$. For $\rho = 0$, the pulse is a hyperbolic secant, and for $\rho = 1$, the pulse is square.

It is easy to see that in the nonlinear Fourier integral [Eq. (7)], the contribution of the flat-top is simply proportional to

$$A_0\, e^{i\chi A_0^2 \eta} \int_0^{\theta} (\hat{x} \sin\phi + \hat{y} \cos\phi) \exp\left[i\chi (1+A_0^2)\right] d\phi, \qquad (9)$$

where the factor $1+A_0^2$ corresponds to the relativistic Doppler shift due to the slower axial motion of the electron caused by the constant laser radiation pressure. The integral in Eq. (9) yields a *sinc* spectrum. Clearly, for $\theta \gg \eta$, the line at the normalized Doppler-shifted frequency $\chi^* = 1/(1+A_0^2)$ dominates the backscattered spectrum, as shown in Fig. 2 (right). The shorter wavelength lines correspond to a combination of the multiphoton lines resulting from the nonlinear Doppler shift during the transient parts of the pulse and the oscillations of the *sinc*.

The beneficial effects of square optical pulses, which can be generated by holographic filtering at the Fourier plane of a CPA laser,[18] can be evaluated quantitatively by considering the evolution of the ratio of the energy in the main line to the total backscattered energy, as a function of the pulse shape. The results are shown in Fig. 3, clearly validating the pulse shaping approach at ultrahigh intensities, and demonstrating that square optical pulses correspond to the optimum shape for Compton backscattering applications.

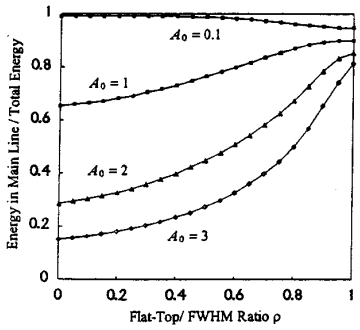

Fig. 3 Energy contrast ratio as a function of pulse shape for various intensities.

Colliding Laser Pulses.

Next, we suggest a new idea to produce extremely short wavelength photons, in which vacuum ponderomotive acceleration (VPA) is combined with Compton backscattering [Fig. 4 (left)]. In this way, the energy acquired by an electron beam within the drive laser pulse may be effectively extracted in the form of short wavelength photons by a colliding probe laser pulse, without

requiring complex structures to end the interaction, thus preserving the simplicity of VPA,[1] as compared to other laser acceleration schemes. We will show that, in this process, the photon energy scales as $h\nu \cong 4\,(hc/\lambda_0)\,\gamma_0^2 A_0^4$, where λ_0 is the laser wavelength (pump and probe), γ_0 is the initial beam energy, and $A_0 = e\,E_0\,\lambda_0/2\pi\,m_0c^2 = (e\,\lambda_0/\pi\,m_0c^{5/2})\,\sqrt{I_0/2\,\varepsilon_0}$ is the dimensionless amplitude of the 4-vector potential of the drive laser, expressed in terms of the focused intensity I_0.

As an example, 1-TeV photons could be produced with an 8.5×10^{20}W/cm^2 drive pulse at 800 nm, interacting with a 550 MeV beam. These parameters correspond to $A_0 = 20$. The advantageous energy scaling of the interaction results directly from the fact that Compton backscattering occurs when the initial electron energy has been boosted by VPA to its maximum value, given by $\gamma^*/\gamma_0 \simeq A_0$, as shown above.

It is instructive to evaluate the length required by this acceleration process. For a circularly polarized pulse interacting with ultrarelativistic electrons, the nonlinear slippage length is roughly $\Delta z \cong \frac{c}{\omega_0}\int_{\phi_0}^{0}\left[1+A_0^2\,g^2(\psi)\right]d\psi$, where ϕ_0 is the injection phase of the electron. For a *sin*^{4} temporal intensity envelope, which closely matches a Gaussian, with a finite duration $\eta = \omega_0\Delta t$, one finds $\Delta z = \gamma_0^2\,c\,\Delta t\,(1+3A_0^2/8)$. The acceleration length required to yield 1-GeV photons with a drive laser strength of 20 and a duration of 20 fs FWHM is estimated at 2.5 m. This estimate denotes an upper bound, as 3D effects reduce the average laser strength along the electron path.

The next step in the analysis shows that the drive and probe laser pulses are decoupled because of their disparate Doppler shifts. The phase of the counterpropagating probe pulse is $\varphi = t+z$, and the differential phase variation between each pulse evolves along the electron trajectory according to $d_\phi\varphi = (d_\tau\varphi)\,(d_\phi\tau) = (\gamma+u_z)/(\gamma-u_z) \cong \left[\gamma_0(1+\beta_0)\right]^2 \cong 4\,\gamma_0^2$. The last two equalities are valid if the radiation pressure of the probe pulse is much smaller than that of the drive pulse. As a result, the drive laser fields are "frozen" during the interaction between the accelerated electron and the probe pulse. Note that the relation $\boldsymbol{u}_\perp = \boldsymbol{A}_\perp + \boldsymbol{A}_p$ still holds. Here, $\boldsymbol{A}_p$ is the normalized potential of the probe laser. Also, for a linearly polarized drive pulse, the fields are clearly equal to zero at the maximum electron energy, since they are proportional to $d_\phi A_x$ and $A_\perp^2(\phi) = A_x^2(\phi)$. Another benefit of linear polarization is that the transverse position of the electron during backscattering is small: $x(\phi) \cong \frac{c}{\omega_0\kappa_0}\int_{-\infty}^{\phi} u_x(\psi)\,d\psi$, which yields $x^* = x(\phi=0) \cong (\lambda_0/4\sqrt{\pi})\gamma_0(1+\beta_0)\,A_0\,\eta\exp(-\eta^2/4)$ for a Gaussian pulse. But, this equation also indicates that the maximum transverse excursion during VPA can be large: $\sigma_x \cong (\lambda_0/\pi)\gamma_0(1+\beta_0)\,A_0$. This must be considered when defining the dimensions of the slab focus geometry, where the beam cross-section is $\Sigma = \sigma_x\,\sigma_y$, with σ_y chosen as small as possible to minimize the drive pulse energy.

Finally, the angle of the electron trajectory during backscattering, defined by the ratio of the transverse and axial momenta in the drive laser, is small: $\theta^* = \arctan\left[\frac{u_x}{u_z}(\phi=0)\right] \cong A_0/\left\{\gamma_0\left[\beta_0+\frac{1}{2}(1+\beta_0)A_0^2\right]\right\} \cong 1/\gamma_0\,A_0$. Despite its low value, this angle is critical in obtaining the full Doppler upshift for the backscattered radiation. To illustrate this point, it is instructive to compare the Doppler upshift along the z-axis, $(\gamma^*+u^*)/(\gamma^*-u^*) = [(1+\beta_0)/(1-\beta_0)](1+A_0^2) \cong 4\,\gamma_0^2 A_0^2$, which is seen to scale as the square of the drive field, to the full Doppler upshift, $(\gamma^*+u^*)/(\gamma^*-u^*) = \left[\gamma^*(1+\beta^*)\right]^2 \cong 4\,\gamma_0^2 A_0^4$.

The Compton backscattered spectrum is obtained from Eq. (7), by replacing the initial velocity by the maximum velocity due to the drive laser:

$$\frac{d^2N(\varpi,\theta^*)}{d\varpi\,d\Omega} = \frac{a\,\varpi}{4\pi^2}\frac{1-\beta^*}{1+\beta^*}\left|\int_{-\infty}^{+\infty}\boldsymbol{A}_p(\varphi)\exp\left\{i\varpi\left(\frac{1-\beta^*}{1+\beta^*}\right)\left[\varphi+\int_{-\infty}^{\varphi}A_p^2(\psi)\,d\psi\right]\right\}d\varphi\right|^2. \tag{10}$$

In the case of a Gaussian wavepacket, in the linear regime ($A_p^2 \ll 1$), one obtains

$$\frac{d^2N(\varpi,\theta^*)}{d\varpi\,d\Omega} \cong \frac{a}{4\pi^2}\,\frac{A_p^2\,\eta^2}{4\gamma_0^2 A_0^4}\,\varpi\,\exp\left[-\frac{\eta^2}{2}\left(\frac{\varpi}{4\gamma_0^2 A_0^4}-1\right)^2\right], \tag{11}$$

where the backscattered line frequency has the value, $\varpi \cong 4\,\gamma_0^2 A_0^4$. To estimate the total photon yield, Eq. (11) is integrated over all frequencies, to obtain $d_\Omega N(\theta^*) \cong a\,\sqrt{2/\pi^3}\,\gamma_0^2 A_p^2 A_0^4\,\eta$. The solid angle is then replaced by $\Delta\Omega \simeq (\pi/\gamma_0^2 A_0^4)$ to yield the average number of photons scattered by an electron: $N_\gamma/N_e \approx a\sqrt{2/\pi}\,A_p^2\,\eta$.

The overall scaling of the process, for a slab geometry, is sketched in Fig. 4 (right), where the following parameters are fixed: $\lambda_0 = 800$ nm, $\sigma_y = 5\,\lambda_0$, and where the pulse duration is 20 fs FWHM. Using the frequency scaling, the relation between the intensity and the vector potential, and the equation for the transverse excursion, with the constraint that the drive pulse energy $W = I_0\,\sigma_x\,\sigma_y$, the photon energy can be expressed in terms of the electron beam energy, γ_0, and W, as $\frac{h\nu}{e} \propto W^{4/3}\,\gamma_0^{2/3}$, or more accurately, as $\varpi = 4\left(\frac{1}{4\pi^{2/3}}\,\frac{\lambda_0}{\sigma_y}\,\frac{W}{\Pi\,\Delta t}\right)^{4/3}\gamma_0^{2/3}$, where the parameter $\Pi = \varepsilon_0\,m_0^2\,c^5/e^2 = 0.6931$ GW has been introduced.

Finally, the speculative nature of this proposal should be stressed: a conclusive argument for or against the practical feasibility of this physical process as a viable radiation source requires detailed studies of some possible problems, including

coherence, electron beam phase space, 3D and diffraction effects, and radiation losses in parasitic synchrotron radiation channels, all contributing to the final brightness and efficiency of the photon source.

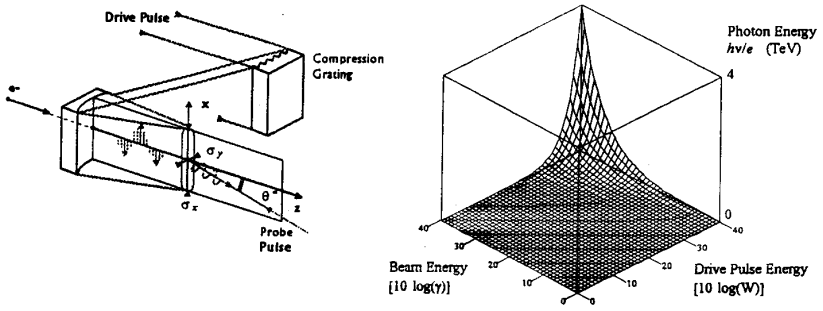

Fig. 4 Left: geometry of the colliding pulses interaction process. Right: photon energy (linear scale) as a function of beam and drive laser energies for a slab geometry. $\lambda_0 = 800$ nm, $\sigma_y = 5\,\lambda_0$, 20 fs FWHM.

Three-Dimensional Dynamics, Ponderomotive Scattering

The Paraxial Propagator

The 3D behavior of the laser electromagnetic field propagating in vacuum is now described in the context of the paraxial propagator formalism. The wave equation governing the 4-vector potential is $\Box A_\mu + 4\pi j_\mu = [\partial_\nu\,\partial^\nu]\,A_\mu + 4\pi j_\mu = 0$, where we have introduced the 4-gradient operator, defined as $\partial_\mu \equiv \frac{\partial}{\partial x^\mu} \equiv (-\partial_t, \nabla)$, and the 4-current density $j_\mu \equiv (\rho, \boldsymbol{j})$. Also, it is important to note that the 4-potential must satisfy the Lorentz gauge condition $\partial_\mu A^\mu = 0$.

In vacuum (no sources), a general solution to the wave equation can be constructed as a Fourier superposition of wavepackets of the form

$$A_\mu(x_\nu) = \left(1/\sqrt{2\pi}^{\,4}\right) \iiiint \tilde{A}_\mu(k_\nu)\, \exp(i\, k_\nu\, x^\nu)\, d^4k, \tag{12}$$

where the 4-wavenumber k_μ satisfies the vacuum dispersion relation, which is also the mass shell condition for the photon field: $\hbar^2\,(k_\mu\, k^\mu) = 0$.

When the laser pulse characteristics are defined at focus ($z = 0$), the field distribution can be obtained in any given z-plane by performing the integral

$$A_\mu(x,y,z,t) = \iiint \frac{\tilde{A}_\mu(k_\perp, \varpi, z=0)}{\sqrt{2\pi}^{\,3}} \exp\left[i \left(\varpi t - k_x x - k_y y - \sqrt{\varpi^2 - \boldsymbol{k}_\perp^2}\; z \right) \right] d^2\boldsymbol{k}_\perp\, d\varpi, \tag{13}$$

where we have introduced the focal spectral density $\tilde{A}_\mu(\boldsymbol{k}_\perp, \varpi, z = 0)$.

This result is easily interpreted: the temporal evolution of each wavepacket is described by the frequency spectrum, while the transverse profile of the laser wave is expressed as an integral over a continuous spectrum of transverse vacuum eigenmodes. The dispersion relation indicates how each transverse component of the wavepacket propagates, thus yielding wavefront curvature and diffraction.

In vacuum, the gauge condition reduces to $\nabla \bullet \boldsymbol{A} = 0$, and is satisfied by requiring that $\boldsymbol{A} = \nabla \times \boldsymbol{G}$. For a linearly polarized Gaussian-elliptical focus, the generating field, $\boldsymbol{G}$, takes the form

$$G(x_\mu) = \hat{y}\, G_y(x_\mu)\,,\; G_y(x,y,z=0,t) = \frac{A_0}{k_0}\, g(t)\, \exp\left[-(x/w_{0x})^2 - (y/w_{0y})^2 \right], \tag{14}$$

where w_{0x} and w_{0y} refer to the beam waist along the x-axis and y-axis, respectively, A_0 is the amplitude of the vector potential at focus, k_0 corresponds to the central laser wavelength, and $g(t)$ is the temporal variation of the laser wave, which can be arbitrary. The propagation integral is now approximated by

$$G_y(x,y,z,t) = \iiint \frac{\tilde{G}_y(k_\perp, z=0, \varpi)}{\sqrt{2\pi}^3} \exp\left\{i\left[\omega t - k_x x - k_y y - \left(\varpi - \frac{k_\perp^2}{2k_0}\right)z\right]\right\} d^2k_\perp \, d\varpi, \tag{15}$$

where the square root factor was Taylor-expanded to second-order around $\varpi = 1$ and $\boldsymbol{k}_\perp = \mathbf{0}$. Clearly, the exact and Taylor-expanded axial phase differ only for large values of $\boldsymbol{k}_\perp$, where the spectral density is vanishingly small. The integrals over $d^2\boldsymbol{k}_\perp$ are tractable, as they are complex Gaussians:[17]

$$G_y(x_\mu) = \frac{A_0\, g(\phi)}{k_0}\left[1+\left(\frac{z}{z_{0x}}\right)^2\right]^{-\frac{1}{4}}\left[1+\left(\frac{z}{z_{0y}}\right)^2\right]^{-\frac{1}{4}} \exp\left\{-\left[\frac{x}{w_x(z)}\right]^2 - \left[\frac{y}{w_y(z)}\right]^2\right\}$$

$$\times \exp\left[i\left\{\frac{1}{2}\arctan\left(\frac{z}{z_{0x}}\right) + \frac{1}{2}\arctan\left(\frac{z}{z_{0y}}\right) - \frac{z}{z_{0x}}\left[\frac{x}{w_x(z)}\right]^2 - \frac{z}{z_{0x}}\left[\frac{y}{w_y(z)}\right]^2\right\}\right], \tag{16}$$

where $w_{x,y}(z) = w_{0x,y}\sqrt{1+(z/z_{0x,y})^2}$, and $z_{0x,y} = \frac{1}{2}k_0 w_{0x,y}^2$ represent the Rayleigh ranges for each f-number.

Ponderomotive Scattering

The vector potential of the focusing wave is shown in Fig. 5. The algorithm developed to model the dynamics of a charge interacting with the 3D laser fields employs the second-order Runge-Kutta method and uses the axial electron phase as the integration variable to handle the nonlinear slippage and the relativistic Doppler shift.

For a laser focus with extremely large f-numbers, excellent agreement is found between the numerical results and the analytic expressions obtained for plane wave dynamics; for smaller values of f, scattering is obtained. To obtain efficient scattering, the electron must be seeded far from focus, so that when it has slipped into the nonlinear temporal phase of the pulse, the focus is reached and the electron interacts with the spatio-temporal maximum of the laser wave. High-energy scattering occurs for intermediate values of the f-numbers: for low values, the focus is too tight and the electron scatters away too early; for very large values, we recover the plane wave interaction. The fact that, for higher initial injection energies, efficient scattering requires larger values of the f-number is not surprising, since the transverse electron excursion scales like $\frac{1}{\kappa} \simeq \frac{1}{\kappa_0} = \gamma_0(1+\beta_0)$. For linear polarization, the largest scattering energies are achieved for $f_x > f_y$.

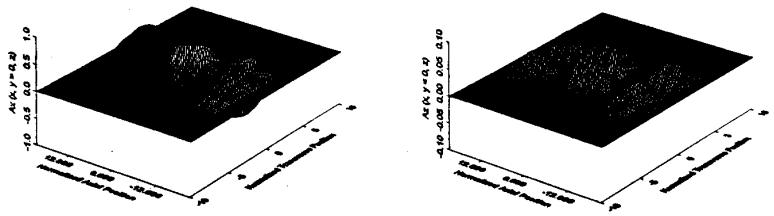

Fig. 5 Transverse and axial vector potential components, in the plane of polarization, at three different times. The pulses are 6 cycles long and f: 3.

To assess the feasibility of laser acceleration based on this process, the total energy in the laser pulse is obtained by integrating the Poynting vector flux over the focal spot and the pulse duration to obtain $\frac{W}{m_0c^2} = \frac{3\pi}{32} A_0^2 \frac{w_{0x}}{\lambda_0}\frac{w_{0y}}{\lambda_0}\frac{c\Delta t}{r_0}$, where r_0 is the classical electron radius. The case of a cylindrical focus ($w_{0x} = w_{0y} = w_0$) is considered, where the pulse FWHM is maintained at 20 fs, and the product $A_0\, w_0$ is kept constant at 250 mm (constant energy of 20 J), while A_0 is varied between 1 and 20, and the injection position is varied between -20 mm and focus. The results are shown in Fig. 6, and clearly indicate the existence of an optimum combination of f-number and laser intensity for high-energy scattering, approximately obtained for a normalized vector potential of 17.5 and f: 23. Here, there is a sharply defined acceptance range in the initial position, and the scattering energy reaches 0.25 GeV. The acceleration process occurs over 3 mm, yielding a gradient of 85 GeV/m. These laser parameters correspond to the next generation of CPA lasers.[19]

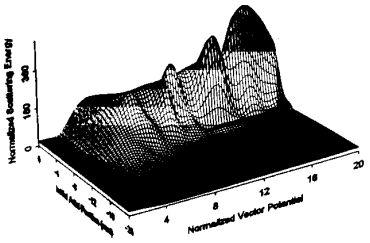

Fig. 6 Scan of A_0 and initial z for a constant pulse energy of 20 J. $\lambda_0 = 1\ \mu$m, FWHM 20 fs, initial energy 10 MeV, $x_i = y_i = 0$.

Dirac-Lorentz Electrodynamics, Radiative Corrections

The Dirac-Lorentz equation[2,8] describes the covariant dynamics of a classical point electron, including the radiation reaction effects due to the electron self-interaction. The main steps of Dirac's derivation are outlined here. For conciseness, we use electron units, where length, time, mass, and charge are measured in units of r_0, r_0/c, m_0, and e, respectively. In these units, $\varepsilon_0 = 1/4\pi$, and $\mu_0 = 4\pi$. The electron 4-current density is $j^s_\mu(x_\lambda) = -\int_{-\infty}^{+\infty} u_\mu(x'_\lambda)\, \delta_4(x_\lambda - x'_\lambda)\, d\tau'$, and the related self-electromagnetic field $F^s_{\mu\nu} = \partial_\mu A^s_\nu - \partial_\nu A^s_\mu$ satisfies the driven wave equation $\Box A^s_\mu(x_\lambda) = 4\pi j^s_\mu(x_\lambda)$, which can be solved using Green functions: $A^s_\mu(x_\lambda) = 4\pi \int_{-\infty}^{+\infty} u_\mu(x'_\lambda)\, G(x_\lambda - x'_\lambda)\, d\tau'$. The self-force can now be evaluated as $F^s_\mu = -\left(\partial_\mu A^s_\nu - \partial_\nu A^s_\mu\right) u^\nu = -\int_{-\infty}^{+\infty} u^\nu(x_\lambda) \left[u_\nu(x'_\lambda)\, \partial_\mu - u_\mu(x'_\lambda)\, \partial_\nu\right] G(x_\lambda - x'_\lambda)\, d\tau'$. The advanced and retarded Green functions both depend on the space-time interval $s^2 = (x - x')_\mu (x - x')^\mu$: $G^\pm = -\delta(s^2)\left[1 \mp (x_0 - x'_0)/|x_0 - x'_0|\right]$. Replacing the partial derivatives by the operator $\partial_\mu \equiv 2\,(x_\mu - x'_\mu)\,\frac{\partial}{\partial s^2}$, the self-force reads

$$F^s_\mu = -2 \int_{-\infty}^{+\infty} u^\nu(x_\lambda) \left[u_\nu(x'_\lambda)\,(x_\mu - x'_\mu) - u_\mu(x'_\lambda)\,(x_\nu - x'_\nu)\right] \frac{\partial G}{\partial s^2}\, d\tau'. \tag{17}$$

Here, the new variable $\tau'' = \tau - \tau'$ is introduced, so that the range of integration explicitly includes the electron (singular point $\tau'' = 0$). To evaluate the integral in Eq. (17), one can now use Taylor-McLaurin expansions in powers of τ'': $x_\mu - x'_\mu = \tau''\, u_\mu - \frac{\tau''^2}{2} a_\mu + \frac{\tau''^3}{6} d_\tau a_\mu + \ldots$ and $u_\mu(x'_\lambda) = u_\mu(\tau - \tau'') = u_\mu - \tau''\, a_\mu + \frac{\tau''^2}{2} d_\tau a_\mu + \ldots$, where the 4-acceleration $a_\mu = d_\tau u_\mu$. Using the above expansions, one first finds that $s^2 \simeq -\tau''^2$, which yields $\frac{\partial G}{\partial s^2} \simeq -\frac{1}{2\tau''} \frac{\partial G}{\partial \tau''}$. With this, the self-electromagnetic force now reads $F^s_\mu \simeq \int_{-\infty}^{+\infty} \left\{-\frac{\tau''}{2}\, a_\mu + \frac{\tau''^2}{3}\,[d_\tau a_\mu - u_\mu\,(a_\nu\, a^\nu)]\right\} \frac{\partial G}{\partial \tau''}\, d\tau''$. This equation can be integrated by parts; using the retarded (causal) Green function, one finds $F^s_\mu = -\frac{1}{2}\, a_\mu \int \frac{\delta(\tau'')}{|\tau''|}\, d\tau'' + \frac{2}{3}[d_\tau a_\mu - u_\mu\,(a_\nu\, a^\nu)]$. The related 4-momentum transfer equation is $\left[1 + \frac{1}{2}\int \frac{\delta(\tau'')}{|\tau''|}\, d\tau''\right] a_\mu = -F_{\mu\nu}\, u^\nu + \tau_0\,[d_\tau a_\mu - u_\mu\,(a_\nu\, a^\nu)]$, where $\tau_0 = 2/3$ is the Compton time-scale, in the units of r_0/c used here. The divergent integral on the left-hand side of the equation is the infinite electromagnetic mass which multiplies the 4-acceleration. Dirac first proposed[8] to renormalize this term away by using the time symmetrical Green function $G = (G^- - G^+)/2$; with this, one obtains the Dirac-Lorentz equation

$$a_\mu = -F_{\mu\nu}\, u^\nu + \tau_0\,[d_\tau a_\mu - u_\mu\,(a_\nu\, a^\nu)]. \tag{18}$$

One problem with this equation is unphysical, runaway solutions: contracting Eq. (18) with a^μ, one can see that, in the absence of an external field, it reduces to $a_\mu\, a^\mu = (\tau_0/2)\, d_\tau(a_\mu\, a^\mu)$, which admits the runaway solution $[a_\mu\, a^\mu](\tau) = [a_\mu\, a^\mu_0]\exp(2\,\tau/\tau_0)$. To avoid these unphysical solutions, one must require that the Dirac-Rohrlich (DR) asymptotic condition[8,20] be satisfied: $\lim_{\tau \to \pm\infty} a_\mu(\tau) = 0$.

Also, note that the second radiative correction term corresponds to the radiated 4-momentum H_μ; thus, we can rewrite Eq. (18) as $a_\mu = -F_{\mu\nu}\, u^\nu + \tau_0\, d_\tau a_\mu - d_\tau H_\mu$. For an external electric field deriving from a static potential, the time-like component of the Dirac-Lorentz equation, which describes energy conservation, takes the form (here, $H_0 = W$) $d_\tau \gamma = \boldsymbol{u} \bullet \nabla\varphi + \tau_0\, d^2_\tau \gamma - d_\tau W = d_\tau\left[\varphi + \tau_0\, d_\tau \gamma - W\right]$, and can be integrated to yield the conservation law $\Delta(\gamma - \varphi + W)$

$= \tau_0 \left[d_\tau \gamma \right]_{-\infty}^{+\infty}$, which indicates that, provided the DR asymptotic condition $\lim_{\tau \to \pm\infty} d_\tau \gamma = 0$ is satisfied, the electron potential energy is converted to kinetic energy and radiation.

In this context, the small value of the fine structure constant, which corresponds to the ratio of the classical to quantum electron scale (classical electron radius divided by the electron Compton wavelength), assures that the acausal effects related to the electromagnetic mass renormalization will be smeared by quantum fluctuations before the strong classical radiative correction regime is reached, thus preventing "naked acausalites".

For nonlinear Compton scattering, the Dirac-Lorentz equation can be given as

$$a_\mu = d_\tau u_\mu = L_\mu + \tau_0 \left[d_\tau a_\mu - u_\mu \left(a_\nu \, a^\nu \right) \right] \, , \; \boldsymbol{L}_\perp = \kappa \, \boldsymbol{E}_\perp \, , \; L_z = L_0 = \boldsymbol{u}_\perp \bullet \boldsymbol{E}_\perp , \tag{19}$$

where we recognize the light-cone variable $\kappa = \gamma - u_z$ and the laser transverse electric field, and $\tau_0 = 2r_0/3c = 0.626 \times 10^{-23}$ s is the Compton time-scale. Subtracting the axial component of Eq. (19) from the temporal component, we obtain an equation governing the evolution of κ,

$$d_\tau \kappa = \tau_0 \left[d_\tau^2 \kappa - \kappa \left(a_\nu \, a^\nu \right) \right] . \tag{20}$$

Noting that $\boldsymbol{E}_\perp = \kappa \, d_\phi \boldsymbol{A}_\perp$, we also obtain an equation governing the evolution of the canonical momentum: $d_\tau (\boldsymbol{u}_\perp - \boldsymbol{A}_\perp) = \tau_0 \left[d_\tau^2 \boldsymbol{u}_\perp - \boldsymbol{u}_\perp \left(a_\nu \, a^\nu \right) \right]$. Introducing the small parameter $\varepsilon = \omega_0 \, \tau_0$, which measures the Doppler-shifted laser wavelength in units of r_0, and using ϕ as the independent variable, Eq. (20) now reads $d_\phi \kappa = \varepsilon \left[d_\phi^2 (\kappa^2/2) - \kappa^2 (d_\phi u_\mu \, d_\phi u^\mu) \right]$. Since the right-hand side of this result is at least of order ε, we can replace the terms in the brackets by their zeroth-order approximation; here, we obtain a simple differential equation for the light-cone variable perturbation $d_\phi \left[\, 1/\kappa(\phi) \, \right] \simeq \varepsilon A_0^2 \, g^2(\phi)$, where we recognize the envelope of the circularly polarized laser pulse. This can easily be integrated to yield $\frac{1}{\kappa(\phi)} = \frac{1}{\kappa_0} + \varepsilon A_0^2 \int_{-\infty}^{\phi} g^2(\psi) \, d\psi$. This equation describes the electron recoil for beam parameters similar to those of SLAC,[6] as illustrated in Fig. 7 (left). It is clear that at sufficient intensities, the relative radiative energy loss becomes significant.

Finally, the Dirac-Lorentz equation can be integrated backward in time to avoid runaways due to the electromagnetic mass renormalization[8,20,21] and the Compton backscattered spectrum is obtained by evaluating

$$\frac{d^2 N(\varpi, -\hat{z})}{d\varpi \, d\Omega} = \frac{a \varpi}{4\pi^2} \left| \int_{-\infty}^{+\infty} \frac{\boldsymbol{u}_\perp(\phi)}{\kappa(\phi)} \exp\left\{ i \, \varpi \left[\phi + 2 \int_{-\infty}^{\phi} \frac{u_z(\psi)}{\kappa(\psi)} \, d\psi \right] \right\} \right|^2 . \tag{21}$$

For the SLAC beam parameters, and a TW-class laser, the result is shown in Fig. 7 (right). At this intensity (0.22 TW/mm^2), the nonlinear Doppler shift yields complex spectra for both Lorentz and Dirac-Lorentz dynamics, but the lines are shifted, analogous to the Lamb shift, and damped at high frequencies.

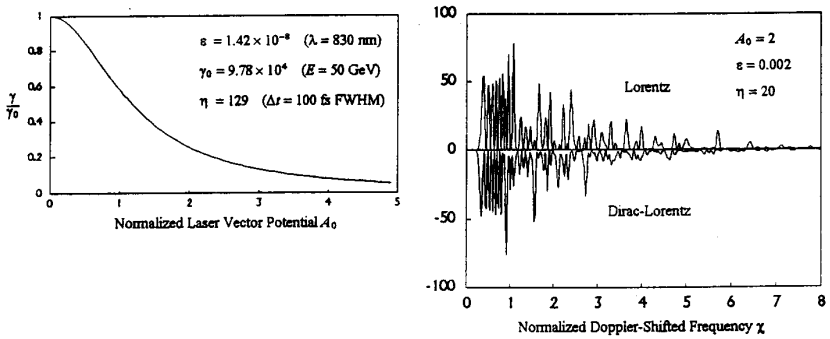

Fig. 7 Left: fractional final electron energy after nonlinear Compton backscattering. Right: Lorentz and Dirac-Lorentz backscattered spectra.

Acknowledgments

This work was partially supported under the auspices of the U.S. Department of Energy by the Lawrence Livermore National Laboratory under contract No. W-7405-ENG-48. This work was also supported in part by DoD/AFOSR (MURI) F49620-95-1-0253, AFOSR (ATRI) F30602-94-2-001, and ARO DAAHO4-95-1-0336. One of us (F.V.H.) wishes to personally thank D.T. Santa Maria for very stimulating discussions.

References

1. F.V. Hartemann *et al.*,Phys. Rev. **E51**, 4833 (1995).
2. F.V. Hartemann and A.K. Kerman, Phys. Rev. Lett. **76**, 627 (1996).
3. F.V. Hartemann, A.L. Troha, N.C. Luhmann, Jr., and Z. Toffano, Phys. Rev. **E54**, 2956 (1996).
4. P.L. Kapitza and P.A.M. Dirac, Proc. Cambridge Philos. Soc. **29**, 297 (1933).
5. P.H. Bucksbaum *et al.*, Phys. Rev. **A41**, 4119 (1990).
6. C. Bula *et al.*, Phys. Rev. Lett. **76**, 3116 (1996).
7. G. Malka, E. Levebvre, and J.L. Miquel, Phys. Rev. Lett. **78**, 3314 (1997).
8. P.A.M. Dirac, Proc. R. Soc. London Ser. **A167**, 148 (1938).
9. J.D. Jackson, *Classical Electrodynamics* (2nd edition, John Wiley and Sons, New York, NY, 1975).
10. C.W. Roberson and P. Sprangle, Phys. Fluids **B1**, 3 (1989).
11. T. Tajima and J.M. Dawson, Phys. Rev. Lett. **43**, 267 (1979).
12. C. Joshi, T. Tajima, J.M. Dawson, H.A. Baldis, and N.A. Ebrahim, Phys. Rev. Lett. **47**, 1285 (1981).
13. D.W. Forslund, J.M. Kindel, W.B. Mori, C. Joshi, and J.M. Dawson, Phys. Rev. Lett. **54**, 558 (1985).
14. W.B. Mori, C. Joshi, J.M. Dawson, D.W. Forslund, and J.M. Kindel, Phys. Rev. Lett. **60**, 1298 (1988).
15. C.E. Clayton *et al.*, Phys. Rev. Lett. **70**, 37 (1993).
16. P. Sprangle, E. Esarey, and J. Krall, Phys. Plasmas **3**, 2183 (1996).
17. I.S. Gradshteyn *et al.*, *Table of Integrals, Series, and Products* (Academic Press, Orlando, FL, 1980).
18. A.M. Weiner, J.P. Heritage, and E.M. Kirschner, J. Opt. Soc. Am. **B5**, 1563 (1988).
19. M.D. Perry and G. Mourou, Science **264**, 917 (1994).
20. F. Rohrlich, *Classical Charged Particles* (Addison-Wesley, Reading, MA, 1965).
21. *Electromagnetism, Paths to Research*, edited by D. Teplitz (Plenum Press, New York and London, 1982), Chaps. 6, by S. Coleman, and 7, by P. Pearle.
22. F.V. Hartemann, Phys. Plasmas **5**, 2037 (1998).